MAJOR PAPER

Comparison between Glioblastoma and Primary Central Nervous System Lymphoma Using MR Image-based Texture Analysis

Akira Kunimatsu[1,2*], Natsuko Kunimatsu[3], Kouhei Kamiya[4], Takeyuki Watadani[4], Harushi Mori[1], and Osamu Abe[1]

Purpose: To elucidate differences between glioblastoma (GBM) and primary central nervous system lymphoma (PCNSL) with MR image-based texture features.

Methods: This was an Institutional Review Board (IRB)-approved retrospective study. Consecutive, pathologically proven, initially treated 44 patients with GBM and 16 patients with PCNSL were enrolled. We calculated a total of 67 image texture features on the largest contrast-enhancing lesion in each patient on post-contrast T_1-weighted images. Texture analyses included first-order features (histogram) and second-order features calculated with gray level co-occurrence matrix, gray level run length matrix (GLRLM), gray level size zone matrix, and multiple gray level size zone matrix. All texture features were measured by two neuroradiologists independently and the intraclass correlation coefficients were calculated. Reproducible features with the intraclass correlation coefficients of greater than 0.7 were used for hierarchical clustering between the cases and the features along with unpaired t statistics-based comparisons under the control of false discovery rate (FDR) < 0.05. Principal component analysis (PCA) was performed to find the predominant features in evaluating the differences between GBM and PCNSL.

Results: Twenty-one out of the 67 features satisfied the acceptable intraclass correlation coefficient and the FDR constraints. PCA suggested first-order entropy, median, GLRLM-based run length non-uniformity, and run percentage as the distinguished features. Compared with PCNSL, run percentage and median were significantly lower, and entropy and run length non-uniformity were significantly higher in GBM.

Conclusions: Among MR image-based textures, first-order entropy, median, GLRLM-based run length non-uniformity, and run percentage are considered to enhance differences between GBM and PCNSL.

Keywords: *magnetic resonance imaging, glioblastoma, primary central nervous system lymphoma, texture analysis*

Introduction

Glioblastoma or glioblastoma multiforme (GBM) is a high grade glioma with predominantly astrocytic differentiation that corresponds to the grade IV by the classification of the central nervous system (CNS) tumors from the World Health Organization (WHO).[1] GBM accounts for approximately 15% of all intracranial neoplasms and is the most frequent malignant brain tumor in adults. GBM preferentially affects adults with a peak incidence between 45 and 75 years with a slight male predominance.

Primary CNS lymphoma (PCNSL) is a nervous-system-seeking, extranodal, non-Hodgkin's lymphoma.[2] It occurs in the brain, meninges, spinal cord, nerve roots, or eyes, and typically remains confined to the CNS. PCNSL accounts for 3.1% of all primary brain neoplasms with a slight male predominance as well. PCNSL most commonly affects adults with the median age of 53 to 57 years at diagnosis of PCNSL in immunocompetent patients.[3]

Despite an approximately 5-fold higher incidence of GBM over PCNSL, GBM and PCNSL share common features in age at presentation and gender predominance; thus, they reasonably include each other in the differential diagnosis. However, treatment strategies substantially differ between GBM and PCNSL. For GBM, maximal tumor

[1]Department of Radiology, Graduate School of Medicine, The University of Tokyo, Tokyo, Japan
[2]Department of Radiology, IMSUT Hospital, The Institute of Medical Science, The University of Tokyo, 4-6-1 Shirokanedai, Minato-ku, Tokyo 108-8639, Japan
[3]Department of Radiology, International University of Health and Welfare, Mita Hospital, Tokyo, Japan
[4]Department of Radiology, The University of Tokyo Hospital, Tokyo, Japan
*Corresponding author, Phone: +81-3-3443-8111, E-mail: akrk-tky@umin.ac.jp

resection followed by radiation therapy and chemotherapy with temozolomide is the current treatment of choice,[4] whereas for PCNSL, stereotactic intracranial biopsy followed by methotrexate-based chemotherapy is usually chosen.[2] Therefore, preoperative differentiation of GBM and PCNSL is of high clinical relevance.[5]

Post-contrast brain MR imaging findings are well-established on GBM and PCNSL: GBM typically exhibits thick, irregular, ring-like or heterogeneous enhancement with central hypo-intense necrosis, whereas PCNSL typically exhibits solid homogeneous enhancement in immunocompetent patients.[6,7] Findings on post-contrast MR images largely contribute to making the preoperative diagnosis. However, this pattern is not reliable in some clinical scenarios because atypical, solid enhancing GBM without visible necrosis may mimic PCNSL, and atypical PCNSL with visible necrosis may mimic GBM in tumor appearance.[5] Therefore, the image-based visual analysis of GBM and PCNSL remains to be improved.

Texture analysis describes a variety of image-analysis techniques that quantify the variation in surface intensity or patterns, including some that are imperceptible to the human visual system.[8] Texture analysis can be applied to a variety of digital images, and thus, is recently attracting increasing interest in the context of future utilization of artificial intelligence in the field of medical imaging. In oncological neuroimaging, recent MR image-based texture analysis studies reported differentiation between radionecrosis from brain tumor recurrence,[9] patient survival in GBM,[10] grading of cerebral gliomas,[11] differentiation of brain metastases from different pathologies,[12] and differentiation of the posterior fossa tumors.[13] To our knowledge, however, there have been no reports on the analysis of GBM and PCNSL with texture features derived from post-contrast MR images. The purpose of this study was to elucidate the differences between GBM and PCNSL using post-contrast MR image-based texture features.

Materials and Methods

Subjects

We first performed a database search on our radiology report up to August 2015. The search criteria were 1) initial case of pathologically proven GBM or CNS lymphoma, and 2) contrast-enhanced brain MRI performed on a 3-T unit with our brain tumor imaging protocol before surgical operation or biopsy. Initially, 52 consecutive patients with GBM and 18 consecutive patients with CNS lymphoma, from December 2006 through August 2015, fulfilled these inclusion criteria. Pathological diagnosis was based on the WHO 2007 classification, as the WHO revised the classification in 2016.

However, 8 of the 52 patients with GBM were excluded due to presence of motion artifacts ($n = 5$), non-enhancing tumor ($n = 1$), history of previous surgery for diffuse astrocytoma ($n = 1$), and protocol violation ($n = 1$).

All of the CNS lymphomas were diffuse large B-cell subtype that developed in immunocompetent patients. Two patients with concurrent CNS involvement of systemic lymphoma were excluded. Neither AIDS-related nor Epstein-Barr virus-related lymphoma was included in our case cohort.[14]

Finally, 44 GBM patients (30 men and 14 women; mean age: 61.5 years, range 26 to 81) and 16 PCNSL patients (13 men and 3 women, mean age: 60.6 years, range 42 to 75) were included in this study (Fig. 1).

MR imaging

Using the picture archiving and communication system of our hospital, post-contrast trans-axial spin-echo T_1-weighted images were retrieved from MR images obtained with our 3-T brain tumor protocol. All MR images were obtained on a 3-T system (Signa HDx, system versions of 14 and of 15 after system software upgrade, GE Healthcare UK Ltd, Little Chalfont, England) and imaging parameters were as follows: TR/TE (ms) = 400/minimum, FOV = 21.0 cm, matrix = 256 × 256, slice thickness = 5 mm. All patients received one of the following gadolinium-based contrast agents at the rate of 0.1 mmol/kg body weight: gadopentetate dimeglumine (Magnevist, Bayer Yakuhin, Ltd., Osaka, Japan), gadodiamide hydrate (Omniscan, Daiichi Sankyo Co., Ltd., Tokyo, Japan), gadoteridol (ProHance, Eisai Co., Ltd., Tokyo, Japan), or gadoterate meglumine (Magnescope, Fuji Pharma Co., Ltd., Tokyo, Japan).

Image analysis

First, a post-contrast T_1-weighted image that harbored the largest contrast-enhancing lesion was selected for each case.
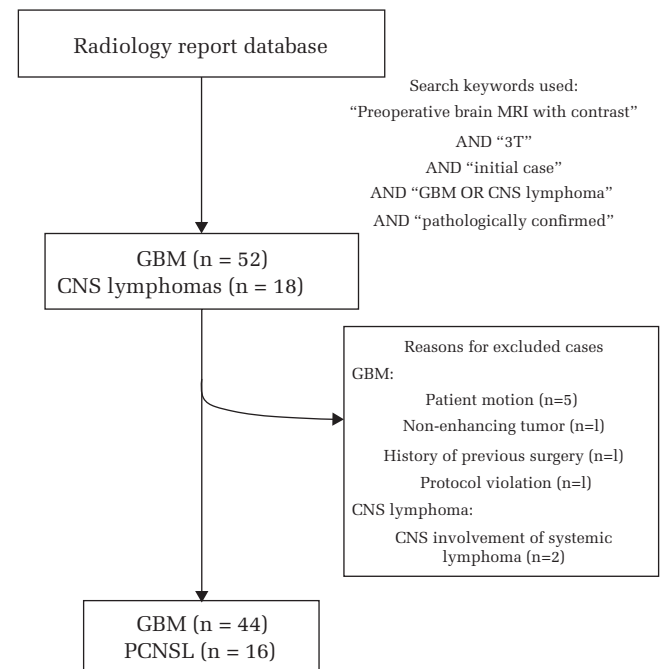

Fig. 1 Flow chart of subject enrollment. GBM, glioblastoma; CNS, central nervous system; PCNSL, primary central nervous system lymphoma.
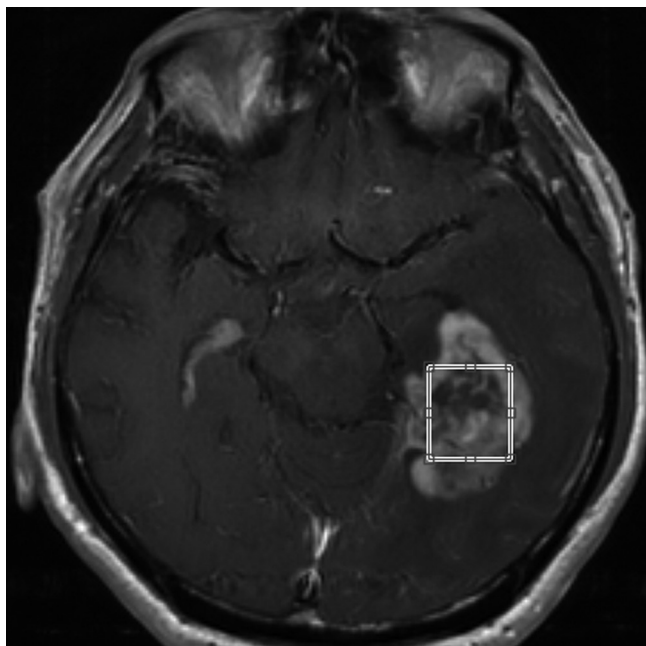
Fig. 2 Pretreatment post-contrast T_1-weighted image of a 68-year-old man subsequently diagnosed with glioblastoma. Post-contrast T_1-weighted image shows a heterogeneously enhanced tumor in the left medial temporal lobe. A rectangular region of interest is placed on the tumor.

The images in the Digital Imaging and COmmunication in Medicine (DICOM) format were converted to 8-bit images using image processing software (ImageJ 1.48, National Institute of Health, Bethesda, USA, http://imagej.nih.gov/ij) along with intensity standardization. Then, using numerical analysis software (MATLAB 2014a, The Mathworks, Tokyo, Japan), the anonymized image was shown and a rectangular ROI was carefully placed within the enhancing lesion as large as possible independently by two neuroradiologists with 20 and 21 years of experience, respectively (Fig. 2). All voxel values within the rectangular ROI were recorded.

Image texture feature extraction

We used software for statistical computing and graphics (R 3.1.2, The R Foundation for Statistical Computing, Vienna, Austria, https://cran.r-project.org/) for texture feature calculation. We obtained first-order texture features and second-order features calculated with gray level co-occurrence matrix (GLCM), gray level run length matrix (GLRLM), gray level size zone matrix (GLSZM), and multiple gray level size zone matrix (mGLSZM),[15] provided in the radiomics package (Joel Carlson [2016]. radiomics: Radiomic Image Processing Toolbox, R package version 0.1.2.). A displacement vector with the distance of one was set at typical angle of 0, 45, 90, and 135 degrees, and the corresponding values were averaged such that GLCM and GLRLM became rotationally invariant. A total set of 67

texture features after standardization (z-scoring) were extracted for each case (Table 1).

Statistical analyses

After the Kolmogrov-Smirnov test for normality, the intraclass correlation coefficient (ICC) was measured with the two-way random model to evaluate the interobserver reproducibility.[16] An intraclass correlation coefficient of greater than 0.7 was considered reliable according to the literature,[17,18] and the features with the coefficients above 0.7 were included in the following analyses after averaging.

Hierarchical clustering was performed using Ward's method. We explored which texture features significantly differed between GBM and PCNSL with unpaired t statistics-based multiple comparisons, provided by the OCplus package under the control of false discovery rate (FDR) < 0.05 (Yudi Pawitan and Alexander Ploner [2016]. OCplus: Operating characteristics plus sample size and local fdr for microarray experiments. R package version 1.48.2.).

Finally, principal component analysis (PCA) was performed to find the predominant features from among highly correlated features with one another.

All statistical analyses were performed with MATLAB and R packages.

Results

Results of ROI measurement and reproducibility

The median size of the ROIs placed by the radiologists was 413.8 mm^2 with the interquartile range of 204.9–658.6 mm^2.

The box-whisker plot (Fig. 3) shows the distribution of the intraclass correlation coefficients. The median of the intraclass correlation coefficients was 0.74. Twenty-eight texture features demonstrated the intraclass correlation coefficients above 0.7 (Table 2): 11 first-order features, 7 GLCM features, 3 GLRLM features, 3 GLSZM features, and 4 mGLSZM features. In particular, six first-order features showed an intraclass correlation coefficient larger than 0.9. This may indicate that first-order features are more robust and reproducible due to simplicity of calculation, compared with second-order matrix features.

Hierarchical clustering

On the heat map presentation of hierarchical clustering (Fig. 4), the cases (columns) could be divided into two main clusters. The vertical dendrogram showed that the lower half cluster was comprised of 27 GBMs and 2 PCNSLs. This cluster suggested relatively high values of features 2 (entropy), 4 (mean deviation), 5 (skewness), 9 (max), 13 (standard deviation), 26 (homogeneity), 27 (homogeneity 2), 41 (run length non-uniformity), 48 (small area emphasis), and 59 (multiple gray level intensity variability), localized in the left cluster of the horizontal dendrogram (features). On the other hand, the upper half cluster included 17 GBMs and 14 PCNSLs, which may be

Table 1. MR imaging-based texture features included in this study

Feature no	Texture feature	Feature no	Texture feature
	First-order texture		**Gray level run length matrix features**
1	Energy	35	Gray level non-uniformity
2	Entropy	36	High-gray level run emphasis
3	Kurtosis	37	Long run emphasis
4	Mean deviation	38	Long run high-gray level emphasis
5	Skewness	39	Long run low-gray level emphasis
6	Uniformity	40	Low-gray level run emphasis
7	Mean	41	Run length non-uniformity
8	Median	42	Run percentage
9	Max	43	Short run emphasis
10	Min	44	Short run high-gray level emphasis
11	Variance	45	Short run low-gray level emphasis
12	Root mean square		**Gray level size zone matrix features**
13	Standard deviation	46	Small area emphasis
	Gray level co-occurrence matrix features	47	Large area emphasis
14	Mean	48	Intensity variability
15	Variance	49	Size zone variability
16	Autocorrelation	50	Zone percentage
17	Cluster prominence	51	Low-intensity emphasis
18	Cluster shade	52	High-intensity emphasis
19	Cluster tendency	53	Low-intensity small area emphasis
20	Contrast	54	High-intensity small area emphasis
21	Correlation	55	Low-intensity large area emphasis
22	Difference entropy	56	High-intensity large area emphasis
23	Dissimilarity		**Multiple gray level size zone matrix features**
24	Energy	57	Multiple gray level small area emphasis
25	Entropy	58	Multiple gray level large area emphasis
26	Homogeneity	59	Multiple gray level intensity variability
27	Homogeneity 2	60	Multiple gray level size zone variability
28	Inverse difference moment (normalized)	61	Multiple gray level zone percentage
29	Inverse difference (normalized)	62	Multiple gray level low-intensity emphasis
30	Inverse variance	63	Multiple gray level high-intensity emphasis
31	Maximum probability	64	Multiple gray level low-intensity small area emphasis
32	Sum average	65	Multiple gray level high-intensity small area emphasis
33	Sum entropy	66	Multiple gray level low-intensity large area emphasis
34	Sum variance	67	Multiple gray level high-intensity large area emphasis

subdivided into two clusters characterized by the middle or the right cluster of the horizontal dendrogram. Approximately, one-third of the local cluster corresponded to PCNSL where features 22 (difference entropy), 25 (entropy), 42 (run percentage), 43 (short run emphasis), 46 (small area emphasis), 50 (zone percentage), and 57 (multiple gray level small area emphasis) were relatively high. The most upper-right cluster had 4 GBMs and 9 PCNSLs,

exhibiting relatively high values in features 16 (autocorrelation), 32 (sum average), 34 (sum variance), 63 (multiple gray level high intensity emphasis), and 65 (multiple gray level high intensity small area emphasis). Among them, however, features 9 (max), 22 (difference entropy), 46 (small area emphasis), 50 (zone percentage), and 57 (multiple gray level small area emphasis) did not satisfy the FDR constraint (Table 2).
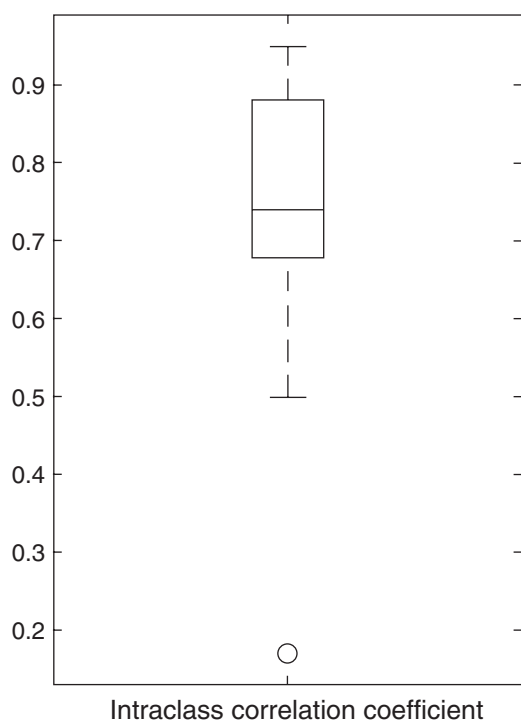
Fig. 3 The box-whisker plot of the intraclass correlation coefficients. The box indicates interquartile range, and the whiskers indicate range, excluding outliers. The circle represents an outlier, defined as having a distance greater than 1.5-times the interquartile range below the first quartile or above the third quartile. The horizontal line in the box represents the median.

Principal component analysis (PCA)

Principal component analysis showed that four principal components reasonably (cumulative percentage contribution > 80%) explained the variance of the feature set: features 42 (run percentage), 8 (median), 2 (entropy), and 41 (run length non-uniformity), in descending order of the percentage contribution. Features 42 (run percentage) and 8 (median) were significantly lower in GBM than in PCNSL, whereas features 2 (entropy) and 41 (run length non-uniformity) were significantly higher in GBM than in PCNSL (Table 2).

Discussion

The differentiation between GBM and PCNSL is important because the appropriate treatments are substantially different. However, differential diagnosis based on interpretation of conventional MR images may be sometimes challenging because atypical, solid enhancing GBM without visible necrosis may mimic PCNSL, and atypical PCNSL with visible necrosis may mimic GBM. Previous studies reported the usefulness of advanced MR imaging, including quantitative diffusion-, perfusion-, and susceptibility-weighted imaging or multiparametric combination of them, for the differentiation between GBM and PCNSL.[5,19–21] To the best of our knowledge, this is the first study focusing on

the difference between post-contrast T_1-weighted images of GBM and PCNSL using a radiomics approach.

As is shown in Fig. 4, the expression patterns of post-contrast MR image-based texture features may vary considerably, not only between the entities (GBM and PCNSL), but also within the single entity (GBM or PCNSL). Some features can be shared between GBM and PCNSL. However, other features can be preferentially striking in GBM compared with PCNSL, and vice versa. For instance, from our results, PCNSL may exhibit high values in feature 32 (sum average) and feature 63 (multiple gray level high intensity emphasis). The rise of these values may be consistent with typical strong contrast enhancement (high voxel intensity) of PCNSL. Features 4 (mean deviation) and 13 (standard deviation) demonstrated positive z-scores in nearly half of GBMs, whereas most PCNSLs demonstrated negative z-scores. This may be explained by greater image heterogeneity (larger deviation of voxel intensity) of GBM compared with PCNSL. Interestingly, features 26 (homogeneity) and 27 (homogeneity 2), enhancing local gray level homogeneity, showed higher values in some GBMs than in PCNSLs.

PCA suggested features 2 (entropy), 8 (median), 41 (run length non-uniformity), and 42 (run percentage) as the predominant (characteristic) features of our data set. The former two are first-order (histogram) features and the latter two are GLRLM features. Entropy quantifies the homogeneity of the image, indicating homogeneous regions with lower entropy values.[10] GLRLM features indicate the coarseness of a texture in a predetermined direction.[8] Run length non-uniformity indicates the similarity of the length of runs throughout the image, which shows low if the run lengths are alike. Run percentage indicates the homogeneity and the distribution of runs of an image in a given direction. For example, the run percentage is very high if the all gray levels have runs with a length of one.[15] Features 2 (entropy) and 41 (run length non-uniformity) showed higher values in GBM than in PCNSL (Table 2). This suggests that GBM may show lower homogeneity and lower similarity of the images than PCNSL. On the other hand, features 8 (median) and 42 (run percentage) showed lower values in GBM than in PCNSL. Necrosis in GBM may reasonably explain the lower median value of the images. Our run percentage results may represent lower image homogeneity in GBM compared with PCNSL.

Radiomics refers to the extraction and analysis of large amounts of advanced quantitative imaging features with high throughput from medical images.[22] The potential of radiomics to contribute for decision support in oncology is growing. Quantitative image features based on intensity, shape, size or volume, and texture offer information on tumor phenotype and microenvironment that are distinct from that provided by standard clinical reports and laboratory test results.[23] A recent study on GBM reported that GLCM-derived homogeneity, angular second moment, inverse difference moment, and entropy from the contrast-enhancing lesion were significantly correlated with overall survival of

Table 2. Interobserver reproducibility and comparison results between feature expressions of GBM and PCNSL

Feature no	Texture feature	Reproducibility ICC (95% CI)	Comparison§ *t*-value
	First-order texture features		
2	Entropy	0.88 (0.80–0.92)	3.41*
3	Kurtosis	0.74 (0.60–0.83)	−2.10*
4	Mean deviation	0.94 (0.91– 0.97)	3.05*
5	Skewness	0.73 (0.59–0.83)	0.69*
6	Uniformity	0.86 (0.78–0.91)	−2.52*
7	Mean	0.95 (0.92–0.97)	−2.05*
8	Median	0.94 (0.90–0.96)	−1.97
9	Max	0.95 (0.91–0.97)	1.33
10	Min	0.71 (0.56–0.82)	−3.59*
12	Root mean square	0.95 (0.91–0.97)	−1.75
13	Standard deviation	0.93 (0.88–0.96)	3.16*
	Gray level co-occurrence matrix features		
16	Autocorrelation	0.71 (0.55–0.82)	−2.81*
22	Difference entropy	0.73 (0.59–0.83)	−0.97
25	Entropy	0.73 (0.58–0.83)	0.77*
26	Homogeneity	0.73 (0.58–0.83)	1.71*
27	Homogeneity 2	0.72 (0.57–0.82)	1.68*
32	Sum average	0.74 (0.61–0.84)	−2.95*
34	Sum variance	0.72 (0.57–0.82)	−2.87*
	Gray level run length matrix features		
41	Run length non-uniformity	0.95 (0.91–0.97)	2.54*
42	Run percentage	0.77 (0.65–0.86)	−2.11*
43	Short run emphasis	0.74 (0.60–0.84)	−1.66*
	Gray level size zone matrix features		
46	Small area emphasis	0.76 (0.63–0.85)	−0.82
48	Intensity variability	0.95 (0.92–0.97)	2.12*
50	Zone percentage	0.77 (0.65–0.86)	−1.30
	Multiple gray level size zone matrix features		
57	Multiple gray level small area emphasis	0.78 (0.66–0.86)	−0.98
59	Multiple gray level intensity variability	0.95 (0.92–0.97)	2.26*
63	Multiple gray level high intensity emphasis	0.79 (0.68–0.87)	−3.43*
65	Multiple gray level high intensity small area emphasis	0.85 (0.76–0.91)	−3.44*

§Comparisons are made between glioblastoma (GBM) and primary central nervous system lymphoma (PCNSL). A positive *t*-value means that the texture shows a higher value in GBM than in PCNSL, and a negative *t*-value means that the texture shows a lower value in GBM than in PCNSL. *indicates that the texture feature satisfies the false discovery rate constraint. ICC, intraclass correlation coefficient; CI, confidence interval.

GBM patients.[10] All of these four features assess the image homogeneity calculated with the formulas that are somewhat alike but somewhat different from one another.

The present study worked on the difference of image texture features between GBM and PCNSL, using post-contrast MR image intensity and texture, but not with shape, size, or volume. Image shape and volume analysis requires accurate and precise delineation of lesion boundaries for segmentation. Manually-traced segmentations by experts are often used as a gold standard or ground truth, but manual segmentation is known as labor-intensive and error-prone.[22] In this study, we cropped a rectangular ROI on the largest contrast-enhancing lesion in each case because we needed to calculate dozens of 2D matrix-based texture features that require a rectangular voxel intensity set of the image, and thus we consider placement of a rectangular ROI is practical.
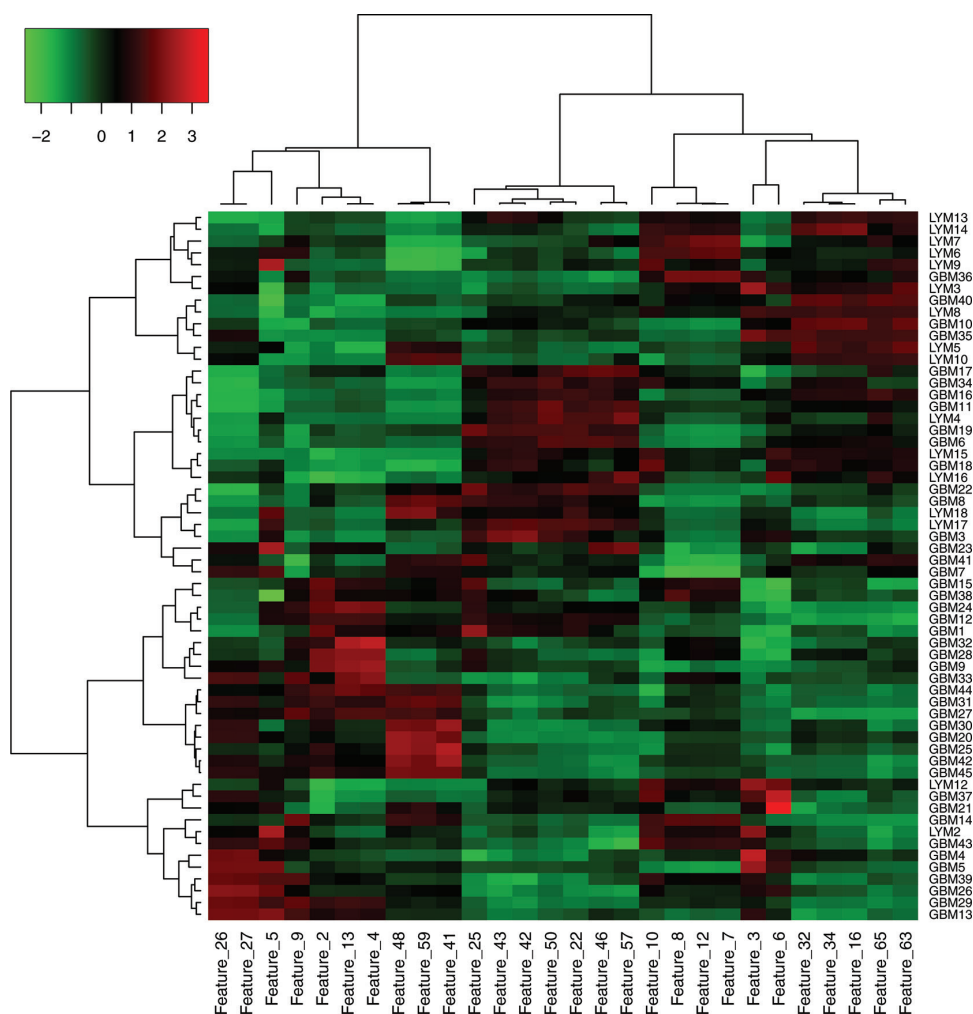
Fig. 4 Hierarchical clustering between the texture features and the cases. The heatmap presentation with dendrograms shows how a texture feature expresses itself among the cases. Red indicates that the texture feature demonstrates a large positive z-score and green indicates that the texture feature demonstrates a large negative z-score. Each row of the heat map represents a specific texture feature across patients, and each column represents all features for a tumor. GBM, glioblastoma; LYM, primary central nervous system lymphoma.

It is also less laborious than manually tracing the lesion boundary by multiple clicks on a computer monitor. In addition, only reproducible measures were taken into the following analyses after the calculation of the ICC.

The current WHO 2016 classification of CNS tumors has adopted a combined molecular-histological classification; thus, pathological diagnosis based on genetic alterations of a tumor is expected to become increasingly available in clinical practice. It is now widely accepted that the prognosis of GBM depends on genetically classified subtypes (24). As this retrospective study included GBM cases diagnosed before the WHO 2016 classification was published, the pathological diagnosis was based on conventional histology. Future works are encouraged on how genetic subtypes of GBM correlate with image texture features.

Our study has some limitations. First, this was a retrospective study with a small number of patients at a single institution, which may have led to bias in patient selection. However, we enrolled consecutive patients who had been studied with the same MR imaging protocols on an identical MR system; therefore, data instability or bias derived from MR scanners and protocols would be minimized.

Second, some texture features did not follow the normal distribution, and were thus excluded from the calculation of the ICC and PCA. ICC and PCA may have been used without mentioning the normality of measurements in the literature, although they assume the normal distribution of samples.[18] Third, in the present study, we did not make a comparison between results with texture analysis and those with the human visual assessment. It remains unclear whether texture analysis can outperform the visual assessment by radiologists. Finally, our study needed to exclude non-enhancing GBM, a rare imaging variant. Texture analysis on T_2-weighted or fluid attenuated inversion recovery (FLAIR) images may be better when including non-enhancing GBM.

Conclusion

MR image-based texture analysis may be a promising tool for differential diagnosis between GBM and PCNSL, although expression patterns of texture features are partly shared between GBM and PCNSL. Among the texture features, first-order entropy, median, GLRLM run length non-uniformity,

and run percentage may be characteristic and most efficiently indicate differences between GBM and PCNSL.

Ethics Statement

This retrospective study was approved by the institutional review board and informed consent was waived.

Conflicts of Interest

The authors declare that they have no conflicts of interest.

References

1. Louis DN, Ohgaki H, Wiestler OD, Cavenee WK (Eds). WHO classification of tumours of the central nervous system. Revised 4th ed. International Agency for Research on Cancer (IARC); Lyon 2016.
2. Hochberg FH, Baehring JM, Hochberg EP. Primary CNS lymphoma. Nat Clin Pract Neurol 2007; 3:24–35.
3. Batchelor T, Loeffler JS. Primary CNS lymphoma. J Clin Oncol 2006; 24:1281–1288.
4. Stupp R, Mason WP, van den Bent MJ, et al. European organisation for research and treatment of cancer brain tumor and radiotherapy groups; national cancer institute of Canada clinical trials group. Radiotherapy plus concomitant and adjuvant temozolomide for glioblastoma. N Engl J Med 2005; 352:987–996.
5. Kickingereder P, Wiestler B, Sahm F, et al. Primary central nervous system lymphoma and atypical glioblastoma: multiparametric differentiation by using diffusion-, perfusion-, and susceptibility-weighted MR imaging. Radiology 2014; 272:843–850.
6. Koeller KK, Smirniotopoulos JG, Jones RV. Primary central nervous system lymphoma: radiologic-pathologic correlation. Radiographics 1997; 17:1497–1526.
7. Rees JH, Smirniotopoulos JG, Jones RV, Wong K. Glioblastoma multiforme: radiologic-pathologic correlation. Radiographics. 1996; 16:1413–1438; 1462–1463.
8. Kassner A, Thornhill RE. Texture analysis: a review of neurologic MR imaging applications. AJNR Am J Neuroradiol 2010; 31:809–816.
9. Tiwari P, Prasanna P, Wolansky L, et al. Computer-extracted texture features to distinguish cerebral radionecrosis from recurrent brain tumors on multiparametric MRI: a feasibility study. AJNR Am J Neuroradiol 2016; 37:2231–2236.
10. Lee J, Jain R, Khalil K, et al. Texture feature ratios from relative CBV maps of perfusion MRI are associated with patient survival in glioblastoma. AJNR Am J Neuroradiol 2016; 37:37–43.
11. Skogen K, Schulz A, Dormagen JB, Ganeshan B, Helseth E, Server A. Diagnostic performance of texture analysis on MRI in grading cerebral gliomas. Eur J Radiol 2016; 85:824–829.
12. Li Z, Mao Y, Li H, Yu G, Wan H, Li B. Differentiating brain metastases from different pathological types of lung cancers using texture analysis of T1 postcontrast MR. Magn Reson Med 2016; 76:1410–1419.
13. Rodriguez Gutierrez D, Awwad A, Meijer L, et al. Metrics and textural features of MRI diffusion to improve classification of pediatric posterior fossa tumors. AJNR Am J Neuroradiol 2014; 35:1009–1015.
14. Lee HY, Kim HS, Park JW, Baek HJ, Kim SJ, Choi CG. Atypical imaging features of Epstein-Barr virus-positive primary central nervous system lymphomas in patients without AIDS. AJNR Am J Neuroradiol 2013; 34:1562–1567.
15. Parmar C, Rios Velazquez E, Leijenaar R, et al. Robust radiomics feature quantification using semiautomatic volumetric segmentation. PLoS ONE 2014; 9:e102107. doi.org/10.1371/journal.pone.0102107.
16. Bartko JJ. On various intraclass correlation reliability coefficients. Psychological Bull. 1976; 83:762–765.
17. Anvari A, Halpern EF, Samir AE. Statistics 101 for radiologists. Radiographics 2015; 35:1789–1801.
18. Bartlett JW, Frost C. Reliability, repeatability and reproducibility: analysis of measurement errors in continuous variables. Ultrasound Obstet Gynecol 2008; 31:466–475.
19. Doskaliyev A, Yamasaki F, Ohtaki M, et al. Lymphomas and glioblastomas: differences in the apparent diffusion coefficient evaluated with high b-value diffusion-weighted magnetic resonance imaging at 3T. Eur J Radiol 2012; 81:339–344.
20. Toh CH, Wei KC, Chang CN, Ng SH, Wong HF. Differentiation of primary central nervous system lymphomas and glioblastomas: comparisons of diagnostic performance of dynamic susceptibility contrast-enhanced perfusion MR imaging without and with contrast-leakage correction. AJNR Am J Neuroradiol 2013; 34:1145–1149.
21. Wang S, Kim S, Chawla S, et al. Differentiation between glioblastomas, solitary brain metastases, and primary cerebral lymphomas using diffusion tensor and dynamic susceptibility contrast-enhanced MR imaging. AJNR Am J Neuroradiol 2011; 32:507–514.
22. Kumar V, Gu Y, Basu S, et al. Radiomics: the process and the challenges. Magn Reson Imaging 2012; 30:1234–1248.
23. Gillies RJ, Kinahan PE, Hricak H. Radiomics: images are more than pictures, they are data. Radiology 2016; 278:563–577.
24. Sanson M, Marie Y, Paris S, et al. Isocitrate dehydrogenase 1 codon 132 mutation is an important prognostic biomarker in gliomas. J Clin Oncol 2009; 27:4150–4154.